A Plane Measuring Device

A.Criminisi, I.Reid and A.Zisserman

Dept. Engineering Science, University of Oxford, Parks Road, Oxford, UK

Abstract

A requirement of a visual measurement device is that both measurements and their uncertainties can be determined. This paper develops an uncertainty analysis which includes both the errors in image localization and the uncertainty in the imaging transformation.

The matrix representing the imaging transformation is estimated from image-to-world point correspondences. A general expression is derived for the covariance of this matrix. This expression is valid if the matrix is over determined and also if the minimum number of correspondences are used. A bound on the errors of the first order approximations involved is also derived.

Armed with this covariance result the uncertainty of any measurement can be predicted, and furthermore the distribution of correspondences can be chosen to achieve a particular bound on the uncertainty. Examples are given of measurements such as distance and parallelism for several applications. These include indoor scenes and architectural measurements.

Key words: Video Metrology; Error Analysis; Projective Geometry.

1 Introduction

The aim of the work in this paper is to be able to make measurements of world planes from their perspective images, and accurately predict the uncertainty of these measurements. Thus a camera becomes a measurement device. Example applications of this device include measurement of interior scenes such as walls or floors for furniture placement and interior design purposes, and architectural measurements, where the size and position of windows, doors etc are determined.

The camera model for perspective images of planes is well known [13]: points on the world plane are mapped to points on the image plane by a *plane to plane homography*, also known as a plane projective transformation. A homography

is described by a 3×3 matrix $\mathtt{H}$. Once this matrix is determined the back-projection of an image point to a point on the world plane is straightforward. The distance between two points on the world plane is simply computed from the Euclidean distance between their back-projected images.

However, a measurement is of little use unless its accuracy is known. Estimating the accuracy (or uncertainty) requires a proper treatment of the sources of error, not just the error in selecting the image points but also the errors in the homography matrix itself. The homography matrix error arises from the position errors of the point correspondences from which the matrix is computed.

In this paper we make three novel contributions: first, it is shown in section 4 that first order uncertainty analysis is sufficient for typical imaging arrangements. This is achieved by developing the analysis to second order and obtaining a bound on the truncation error. Second, it is shown that the first order analysis is exact for the affine part of the homography, and that an approximation is only involved for the non-linear part. Third, in section 5 an expression is obtained for the covariance of the estimated $\mathtt{H}$ matrix by using first order matrix perturbation theory.

The uncertainty analysis developed here builds on and extends previous analysis of the uncertainty in relations estimated from homogeneous equations, for example homographies [11] and epipolar geometry [4,5]. It extends these results because it covers the cases where the matrix is exactly determined *and* the case where the matrix is over-determined, by the world-image correspondences. Furthermore, the anlysis is not adversely affected when the estimation matrix is near singular. This is explained in more detail in section 5. The correctness of the uncertainty predictions has been extensively tested both by Monte Carlo simulation and by numerous experiments on real images.

Sections 6 and 7 describe how the uncertainty analysis is applied to particular measurements taking account of the cumulative effects of different error sources, including the image point localization and the homography matrix covariance.

Section 8 gives examples of predicting uncertainties and achieving a specified uncertainty by varying the number and distribution of correspondences. Both interior and architectural measurement examples are covered.

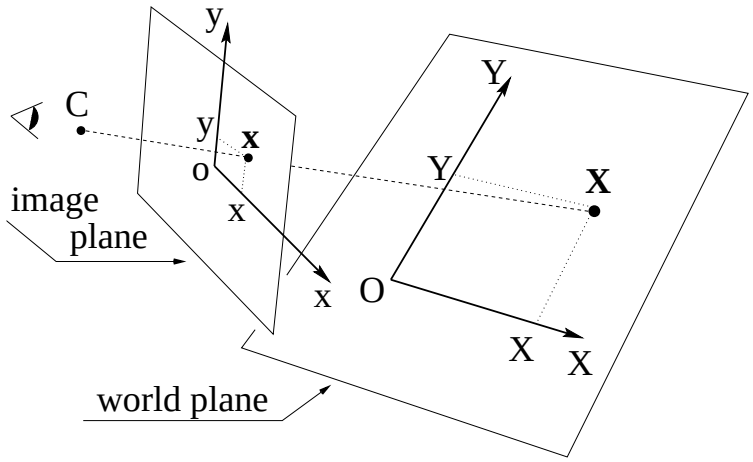


Fig. 1. Plane Camera Model: a point $\mathbf{X}$ on the world plane is imaged as $\mathbf{x}$. Euclidean coordinates XY and xy are used for the world and image planes, respectively. C is the camera centre.

2 The camera model

We describe here the camera model which consists of central projection specialised to planes.

Figure 1 shows the imaging process. The notation used is that points on the world plane are represented by upper case vectors, $\mathbf{X}$, and their corresponding images are represented by lower case vectors $\mathbf{x}$, where $\mathbf{x}$ and $\mathbf{X}$ are homogeneous 3-vectors, $\mathbf{X} = (X, Y, 1)^\top$ and $\mathbf{x} = (x, y, 1)^\top$. Under perspective projection corresponding points are related by [9,13]:

$$\mathbf{X} = \mathtt{H}\mathbf{x} \tag{1}$$

where $\mathtt{H}$ is a 3×3 homogeneous matrix, and "=" is equality up to scale. The camera model is completely specified once the matrix is determined. The matrix can be computed from the relative positioning of the two planes and camera centre. However, it can also be computed directly from image to world point correspondences. This computation is described in the next section.

3 Computing the plane to plane homography

From equation (1) each image to world point correspondence provides two equations linear in the $\mathtt{H}$ matrix elements. They are

$$\begin{aligned} h_{11}x + h_{12}y + h_{13} &= h_{31}xX + h_{32}yX + h_{33}X \\ h_{21}x + h_{22}y + h_{23} &= h_{31}xY + h_{32}yY + h_{33}Y \end{aligned}$$

For n correspondences we obtain a system of $2n$ equation in 8 unknowns. If $n = 4$ then an exact solution is obtained. Otherwise, if $n > 4$, the matrix is over determined, and for non-perfect data `H` is estimated by a suitable minimisation scheme.

The covariance of the estimated `H` matrix depends both on the errors in the position of the points used for its computation *and* the estimation method. There are three standard methods for estimating `H`:

3.1 Non-homogeneous linear solution.

One of the 9 matrix elements is given a fixed value, usually unity, and the resulting simultaneous equations for the other 8 elements are then solved using a pseudo-inverse. This is the most commonly used method. It has the disadvantage that poor estimates are obtained if the chosen element should actually have the value zero.

The most frequent assumption is $h_{33} = 1$. This is not valid if the vanishing line of the world plane intersects the origin of the image coordinate system.

3.2 Homogeneous solution.

The solution is obtained using SVD. This is the method used here and is explained in more detail below. It does not have the disadvantage of the non-homogeneous method.

3.3 Non-linear geometric solution.

The summed Euclidean distances between the measured and a mapped point is minimised. This method has the advantage, over the above two algebraic methods, that the quantity minimised is meaningful and corresponds to the error involved in the measurement (similar minimisations are used to estimate the fundamental matrix and trifocal tensor [15,17]). There is no closed form solution in this case and a numerical minimisation scheme, such as Levenberg-Marquardt [10], is employed. Usually an initial solution is obtained by method 3.2, and then "polished" using the non-linear one.

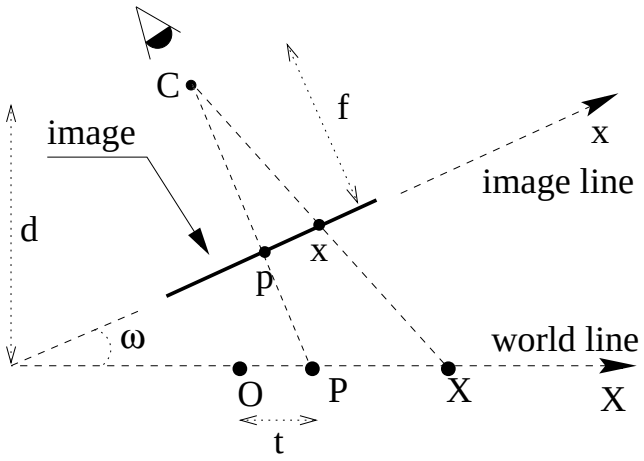


Fig. 2. One-dimensional Camera Model: The camera centre is a distance f (the focal length) from the image line. The ray at the principal point p is perpendicular to the image line, and intersects the world line at P, with world ordinate t. The angle between the world and image lines is ω.

3.4 Homogeneous estimation method

Writing the $\mathtt{H}$ matrix in vector form as $\mathbf{h} = (h_{11}, h_{12}, h_{13}, h_{21}, h_{22}, h_{23}, h_{31}, h_{32}, h_{33})^\top$ the homogeneous equations (1) for n points become $\mathtt{A}\mathbf{h} = \mathbf{0}$, with $\mathtt{A}$ the $2n \times 9$ matrix. Each computation match ($\mathbf{x}_i \leftrightarrow \mathbf{X}_i$) provides two rows of the $\mathtt{A}$ matrix:

$$\begin{pmatrix} x_i & y_i & 1 & 0 & 0 & 0 & -x_iX_i & -y_iX_i & -X_i \\ 0 & 0 & 0 & x_i & y_i & 1 & -x_iY_i & -y_iY_i & -Y_i \end{pmatrix}$$

The vector $\mathbf{h}$ that minimises the algebraic residuals $||\mathtt{A}\mathbf{h}||$, subject to $||\mathbf{h}|| = 1$, is given by the eigenvector of least eigenvalue of $\mathtt{A}^\top\mathtt{A}$. This eigenvector can be obtained directly from the SVD of $\mathtt{A}$. In the case of $n = 4$ the residuals are zero and $\mathbf{h}$ is the null-vector of $\mathtt{A}$.

4 First and second order uncertainty analysis

To avoid unnecessarily complicated algebra the comparison between first and second order analysis is developed for a line to line homography. The one-dimensional case illustrates all the ideas involved, and the algebraic expressions are easily interpreted. The generalisation to 3×3 matrices is straightforward and does not provide any new insights here.

In the one-dimensional case equation (1) reduces to:

$$\begin{pmatrix} X \\ 1 \end{pmatrix} = \mathtt{H}_{2\times 2} \begin{pmatrix} x \\ 1 \end{pmatrix}$$

where $\mathtt{H}_{2\times 2}$ is a 2×2 homography matrix. For the geometry shown in figure 2 the matrix is given by

$$\mathtt{H}_{2\times 2} = \begin{pmatrix} \alpha & t \\ \mu & 1 \end{pmatrix}$$

with parameters $\alpha = \frac{d}{f cos^2(\omega)} - \frac{t}{f} tan(\omega)$ and $\mu = -\frac{tan(\omega)}{f}$.

Under back-projection an image point x maps as

$$x \to X = \frac{h_{11}x + h_{12}}{h_{21}x + h_{22}} = \frac{\alpha x + t}{\mu x + 1}$$

This non-linear mapping (on inhomogeneous coordinates) can be expanded in a Taylor series. Statistical moments of X, such as the variance, are then computed in terms of the Taylor coefficients and the moments of x [2,12]. It is assumed here that the homography is exact (no errors) and the measurement of the image test point x is subject to Gaussian noise with standard deviation σ_x. The Taylor series is developed about the point's mean position denoted as $\bar{x}$.

$$X = \frac{\alpha\bar{x} + t}{\mu\bar{x} + 1} + \frac{\alpha - \mu t}{(\mu\bar{x} + 1)^2}(x - \bar{x}) - \frac{\mu(\alpha - \mu t)}{(\mu\bar{x} + 1)^3}(x - \bar{x})^2 \cdots$$

4.1 First order.

If the Taylor series is truncated to first order in $(x - \bar{x})$ then the mapping is linearised. The variance of X therefore is:

$$\sigma_X^2 = E[(X - \bar{X})^2] \approx E\left[\left(\frac{\alpha - \mu t}{(\mu\bar{x} + 1)^2}(x - \bar{x})\right)^2\right] = \frac{(\alpha - \mu t)^2}{(\mu\bar{x} + 1)^4} E[(x - \bar{x})^2]$$

and since $E[(x - \bar{x})^2] = \sigma_x^2$,

$$\sigma_X^2 \approx \frac{(\alpha - \mu t)^2}{(\mu\bar{x} + 1)^4}\sigma_x^2 \qquad (2)$$

4.2 Second order.

Usually only the first order approximation is used for error propagation [1,4,5,11]. Here we extend the Taylor expansion to second order so that the approximation involved in truncating to first order can be bounded. It can be shown that to second order in $(x - \bar{x})$

$$\sigma_X^2 \approx \frac{(\alpha - \mu t)^2}{(\mu\bar{x} + 1)^4}\sigma_x^2 + \frac{2\mu^2(\alpha - \mu t)^2}{(\mu\bar{x} + 1)^6}\sigma_x^4 \tag{3}$$

We now define two measures that can be used to assess the error in truncating to first order. The first measures the ratio of the second order to first order terms. Comparing equations (2) and (3) this ratio is

$$M_1 = \frac{2\mu^2}{(\mu\bar{x} + 1)^2}\sigma_x^2$$

The second measure, M_2, is obtained from the Lagrange remainder of the Taylor series [14]. This provides an upper bound on the error if the series is truncated to first order instead of using the complete expansion.

From Taylor's Theorem the variance σ_X^2 is

$$\sigma_X^2 = \frac{(\alpha - \mu t)^2}{(\mu\bar{x} + 1)^4}\sigma_x^2 + \frac{2\mu^2(\alpha - \mu t)^2}{(\mu\xi + 1)^6}\sigma_x^4$$

This is the sum of the first order term and the Lagrange remainder, which for some ξ such that $|\bar{x} - \xi| < |\bar{x} - x|$ is an exact equation, not an approximation. The measure M_2 is then obtained as the ratio of this truncation error to the first order term.

$$M_2 = 2\frac{\mu^2(\mu\bar{x} + 1)^4}{(\mu\xi + 1)^6}{\sigma^2}_x$$

and we compute the worst case of $\xi = \bar{x} - \sigma_x$ for this bound in the range $\bar{x} \pm \sigma_x$.

The significance of these measures is that they depend only on the homography matrix elements. Thus, once a matrix has been estimated the need for a second order approximation can be immediately assessed. In typical imaging situations second order terms are not required. For example, if $f = 8.5\,mm$, $d = 5\,m$, $t = 1\,m$, $x = 50\,pixels$, $\sigma_x = 1\,pixel$, and w varies from 45^o to 80^o

(see figure 2) then

w	45^o	60^o	70^o	80^o
M_1	4.7×10^{-6}	1.6×10^{-5}	4.8×10^{-5}	3.7×10^{-4}
M_2	4.7×10^{-6}	1.5×10^{-5}	4.6×10^{-5}	3.5×10^{-4}

4.3 When is first order exact?

If $\mu = 0$ in equation (3) then the second order correction is zero. With $\mu = 0$ the homography reduces to an affine transformation. This illustrates the general result that if the homography is affine the first order analysis is exact.

Generally, the $\mathtt{H}$ matrix can be decomposed into the product of matrices representing *linear* (affine) and *non linear* transformations on inhomogeneous coordinates as: $\mathtt{H} = \mathtt{LP}$ where

$$\mathtt{L} = \begin{pmatrix} \alpha_{11} & \alpha_{12} & h_{13} \\ \alpha_{21} & \alpha_{22} & h_{23} \\ 0 & 0 & 1 \end{pmatrix}, \quad \mathtt{P} = \begin{pmatrix} 1 & 0 & 0 \\ 0 & 1 & 0 \\ h_{31} & h_{32} & 1 \end{pmatrix}, \quad \alpha_{ij} = h_{ij} - h_{3j}h_{i3}. \tag{4}$$

If $\mathtt{H}$ is purely an affinity (linear on inhomogeneous coordinates) then $\mathtt{P}$ is the identity and the first order theory exact.

5 The covariance of the estimated homography

In this section we compute the covariance of the homography $\mathtt{H}$ estimated from n image-world point correspondences. We consider all the computation points to be measured with error modelled as an homogeneous, isotropic Gaussian noise process. For the image computation points we define $\sigma_x = \sigma_y = \sigma$, and for the world ones $\Sigma_X = \Sigma_Y = \Sigma$. It is not strictly necessary to have such idealised distributions but this has not been found to be a restriction in practice.

From section 3.4 we seek the eigenvector $\mathbf{h}$ with smallest eigenvalue λ of $\mathtt{A}^\top\mathtt{A}$. If the measured points are noise-free, or $n = 4$, then $\mathbf{h} = Null(\mathtt{A})$, and in general we can assume that for $\mathbf{h}$ the residual error $\mathbf{h}^\top\mathtt{A}^\top\mathtt{A}\mathbf{h} = \lambda \approx 0$.

We now use matrix perturbation theory [7] to compute the covariance $\Lambda_{\mathbf{h}}$ of $\mathbf{h}$ based on this zero approximation. In a similar manner to [16], it can be shown that the 9×9 covariance matrix $\Lambda_{\mathbf{h}}$ is

$$\Lambda_{\mathbf{h}} = \mathtt{JSJ} \tag{5}$$

where $\mathtt{J} = -\sum_{k=2}^{9} \frac{\mathbf{u}_k \mathbf{u}_k{}^\top}{\lambda_k}$, with $\mathbf{u}_k$ the k^{th} eigenvector of the $\mathtt{A}^\top\mathtt{A}$ matrix and λ_k the corresponding eigenvalue. $\mathtt{S}$ is the 9×9 matrix:

$$\mathtt{S} = \sum_{i=1}^{n} \left(\mathbf{a}_{2i-1}^\top \mathbf{a}_{2i-1} f_i^o + \mathbf{a}_{2i}^\top \mathbf{a}_{2i} f_i^e + \mathbf{a}_{2i-1}^\top \mathbf{a}_{2i} f_i^{oe} + \mathbf{a}_{2i}^\top \mathbf{a}_{2i-1} f_i^{eo} \right)$$

with $\mathbf{a}_i$ the i^{th} row vector of the $\mathtt{A}$ matrix and

$$\begin{aligned} f_i^o = \quad & \sigma^2[h_1^2 + h_2^2 - 2X_i(h_1h_7 + h_2h_8)] + 2\Sigma^2(x_ih_7h_9 + x_iy_ih_7h_8 + \\ & y_ih_8h_9) + (\sigma^2 X_i^2 + x_i^2\Sigma^2)h_7^2 + (\sigma^2 X_i^2 + y_i^2\Sigma^2)h_8^2 + \Sigma^2 h_9^2 \end{aligned}$$

$$\begin{aligned} f_i^e = \quad & \sigma^2[h_4^2 + h_5^2 - 2Y_i(h_4h_7 + h_5h_8)] + 2\Sigma^2(x_ih_7h_9 + x_iy_ih_7h_8 + \\ & y_ih_8h_9) + (\sigma^2 Y_i^2 + x_i^2\Sigma^2)h_7^2 + (\sigma^2 Y_i^2 + y_i^2\Sigma^2)h_8^2 + \Sigma^2 h_9^2 \end{aligned}$$

$$f_i^{oe} = f_i^{eo} = \quad \sigma^2[(h_1 - X_ih_7)(h_4 - Y_ih_7) + (h_2 - X_ih_8)(h_5 - Y_ih_8)]$$

The above theory has a double advantage over other methods such as [1,5] which require the inverse of $\mathtt{A}^\top\mathtt{A}$ in order to compute $\Lambda_{\mathbf{h}}$. These methods are poorly conditioned if only four correspondences are used, or if $n > 4$ and the correspondences are (almost) noise-free. In both cases $\mathtt{A}^\top\mathtt{A}$ matrix is singular and thus is not invertible. Because the derivation of expression (5) has not involved the inverse, it is well conditioned in both these cases.

6 Uncertainty in point localization

There may be errors in the world and image points used to compute the homography, and there may be errors in the image points back projected to make world measurements. All of these uncertainties must be taken into account in order to compute a cumulative uncertainty for the world measurement.

In this section we list the formulae used to compute the uncertainty for measurements under various error situations. The first order analysis is assumed

sufficient. The uncertainty in the homography is computed as described in the previous section.

We first introduce new notation that will simplify the formulae. Equation (1) can be written as $\mathbf{X} = \mathtt{B}\mathbf{h}$, where $\mathtt{B}$ is a 3×9 matrix in the form:

$$\mathtt{B} = \begin{pmatrix} \mathbf{x}^\top & \mathbf{0}^\top & \mathbf{0}^\top \\ \mathbf{0}^\top & \mathbf{x}^\top & \mathbf{0}^\top \\ \mathbf{0}^\top & \mathbf{0}^\top & \mathbf{x}^\top \end{pmatrix} \tag{6}$$

In the following we will determine the 3×3 covariance matrix $\Lambda_{\mathbf{X}}$ of the homogeneous world point $\mathbf{X}$. The conversion to a 2×2 covariance matrix $\Lambda_{\mathbf{X}}^{2\times 2}$ for inhomogeneous coordinates is given by: $\Lambda_{\mathbf{X}}^{2\times 2} = \boldsymbol{\nabla} f \Lambda_{\mathbf{X}} \boldsymbol{\nabla} f^\top$ where $\mathbf{X} = (X, Y, W)^\top$ and

$$\boldsymbol{\nabla} f = 1/W^2 \begin{pmatrix} W & 0 & -X \\ 0 & W & -Y \end{pmatrix}$$

The opposite conversion, from inhomogeneous to homogeneous coordinates, for an image point $\mathbf{x}$ is simply given by:

$$\Lambda_{\mathbf{x}} = \begin{pmatrix} \Lambda_{\mathbf{x}}^{2\times 2} & \mathbf{0} \\ \mathbf{0}^\top & 0 \end{pmatrix}$$

It is easy to prove that, given two homogeneous 3-vectors $\mathbf{x}_1$ and $\mathbf{x}_2$ related by $\mathbf{x}_2 = \lambda \mathbf{x}_1$ with λ a scale factor, and their associated 3×3 covariance matrices Λ_{x_1} and Λ_{x_2}, then $\Lambda_{x_2}^{2\times 2} = \Lambda_{x_1}^{2\times 2}$ where $\Lambda_{x_1}^{2\times 2}$ and $\Lambda_{x_2}^{2\times 2}$ are the corresponding inhomogeneous covariance matrices.

In fact $\Lambda_{x_2} = \lambda^2 \Lambda_{x_1}$ and $\boldsymbol{\nabla} f_2 = \frac{1}{\lambda} \boldsymbol{\nabla} f_1$, therefore

$$\Lambda_{x_2}^{2\times 2} = \frac{1}{\lambda} \boldsymbol{\nabla} f_1 \lambda^2 \Lambda_{x_1} \frac{1}{\lambda} \boldsymbol{\nabla} f_1{}^\top$$

and since $\Lambda_{x_1}^{2\times 2} = \boldsymbol{\nabla} f_1 \Lambda_{x_1} \boldsymbol{\nabla} f_1{}^\top$ then $\Lambda_{x_2}^{2\times 2} = \Lambda_{x_1}^{2\times 2}$.

6.1 Uncertainty in $\mathbf{X}$*, given an uncertain* $\mathtt{H}$ *and exact* $\mathbf{x}$*.*

If we assume noise only on the homography and exact input point $\mathbf{x}$, then the covariance of the corresponding world point is:

$$\Lambda_{\mathbf{X}} = \mathtt{B}\Lambda_{\mathbf{h}}\mathtt{B}^{\top} \tag{7}$$

6.2 Uncertainty in $\mathbf{X}$*, given an exact* $\mathtt{H}$ *and uncertain* $\mathbf{x}$*.*

Instead, if we assume noise only in the input point and an exact homography we get:

$$\Lambda_{\mathbf{X}} = \mathtt{H}\Lambda_{\mathbf{x}}\mathtt{H}^{\top} \tag{8}$$

6.3 Uncertainty in $\mathbf{X}$*, given an uncertain* $\mathtt{H}$ *and uncertain* $\mathbf{x}$*.*

If we assume noise in both the homography $\mathtt{H}$ and the input point $\mathbf{x}$ then the covariance $\Lambda_{\mathbf{X}}$ is given by the sum of the previous two equations (7, 8):

$$\Lambda_{\mathbf{X}} = \begin{pmatrix} \mathtt{B} \vdots \mathtt{H} \end{pmatrix} \begin{pmatrix} \Lambda_{\mathbf{h}} & \vdots & \mathtt{0} \\ \cdots & \cdots & \cdots \\ \mathtt{0} & \vdots & \Lambda_{\mathbf{x}} \end{pmatrix} \begin{pmatrix} \mathtt{B}^{\top} \\ \cdots \\ \mathtt{H}^{\top} \end{pmatrix} \tag{9}$$

In fact $\mathtt{H}$ and $\mathbf{x}$ are statistically independent.

7 Uncertainty in distance measurement

The distance d between two world points $\mathbf{X}_1$ and $\mathbf{X}_2$ will also have an associated uncertainty.

Let the two end points of the image of the segment we want to measure be $\mathbf{x}_1 = (x_1, y_1)^{\top}$ and $\mathbf{x}_2 = (x_2, y_2)^{\top}$

The two corresponding points on the world plane in homogeneus coordinates are: $\mathbf{U}_1 = (U_1, V_1, W_1)^{\top}$ and $\mathbf{U}_2 = (U_2, V_2, W_2)^{\top}$ where $\mathbf{U}_i = \mathtt{H}\,(x_i, y_i, 1)^{\top}$. In inhomogeneus coordinates they are: $\mathbf{X}_i = (X_i, Y_i)^{\top}$ with $X_i = U_i/W_i$ and $Y_i = V_i/W_i$;

The distance between the two points $\mathbf{X}_1$ and $\mathbf{X}_2$ on the world plane is:

$$d = \sqrt{(X_1 - X_2)^2 + (Y_1 - Y_2)^2}$$

and its uncertainty is computed below.

7.1 Uncertainty in d, given an uncertain $\mathtt{H}$ *and exact* $\mathbf{x}_1, \mathbf{x}_2$.

It can be shown that the gradient of d with respect to $\mathbf{h}$ is:

$$\frac{\partial d}{\partial \mathbf{h}} = \frac{1}{d}(\mathbf{X}_1 - \mathbf{X}_2)^\top (\tilde{\mathtt{A}}_1 - \tilde{\mathtt{A}}_2)$$

where the 2×9 matrices $\tilde{\mathtt{A}}_1$ and $\tilde{\mathtt{A}}_2$ are:

$$\tilde{\mathtt{A}}_i = \frac{1}{W_i} \begin{pmatrix} x_i & y_i & 1 & 0 & 0 & 0 & -x_i X_i & -y_i X_i & -X_i \\ 0 & 0 & 0 & x_i & y_i & 1 & -x_i Y_i & -y_i Y_i & -Y_i \end{pmatrix}$$

If we assume noise only in the homography, then, for the first order analysis, the variance of d is given by:

$$\sigma_d^2 = \frac{\partial d}{\partial \mathbf{h}} \Lambda_h \frac{\partial d}{\partial \mathbf{h}}^\top \tag{10}$$

7.2 Uncertainty in d, given exact $\mathtt{H}$ *and uncertain* $\mathbf{x}_1$ *and* $\mathbf{x}_2$.

The gradient of the distance with respect to the 4-vector $\mathbf{z}$ of the input image points $\mathbf{z} = (x_1, y_1, x_2, y_2)^\top$ is given by

$$\frac{\partial d}{\partial \mathbf{z}} = \frac{1}{d}(\mathbf{X}_1 - \mathbf{X}_2)^\top \begin{pmatrix} \mathtt{B}_1 \vdots \mathtt{B}_2 \end{pmatrix}$$

where we have defined the matrices $\mathtt{B}_1$ and $\mathtt{B}_2$ as follows:

$$\mathtt{B}_i = \frac{1}{W_i} \begin{pmatrix} h_{11} - h_{31} X_i & h_{12} - h_{32} X_i \\ h_{21} - h_{31} Y_i & h_{22} - h_{32} Y_i \end{pmatrix}$$

If we assume noise only in the input points $\mathbf{x}_1, \mathbf{x}_2$, then the variance σ_d^2 is

$$\sigma_d^2 = \frac{\partial d}{\partial \mathbf{z}} \begin{pmatrix} \Lambda_{\mathbf{x}_1} & \vdots & 0 \\ \cdots & \cdots & \cdots \\ 0 & \vdots & \Lambda_{\mathbf{x}_2} \end{pmatrix} \frac{\partial d}{\partial \mathbf{z}}^\top \tag{11}$$

7.3 Uncertainty in d, given uncertain H *and uncertain* $\mathbf{x}_1$ *and* $\mathbf{x}_2$.

Finally, if both the homography H and the input points $\mathbf{x}_1, \mathbf{x}_2$ are uncertain then the variance σ_d^2 is given by the sum of the previous two equations (10) and (11):

$$\sigma_d^2 = \begin{pmatrix} \frac{\partial d}{\partial \mathbf{h}} & \vdots & \frac{\partial d}{\partial \mathbf{z}} \end{pmatrix} \begin{pmatrix} \Lambda_{\mathbf{h}} & \vdots & 0 & \vdots & 0 \\ \cdots & \cdots & \cdots & \cdots & \cdots \\ 0 & \vdots & \Lambda_{\mathbf{x}_1} & \vdots & 0 \\ \cdots & \cdots & \cdots & \cdots & \cdots \\ 0 & \vdots & 0 & \vdots & \Lambda_{\mathbf{x}_2} \end{pmatrix} \begin{pmatrix} \frac{\partial d}{\partial \mathbf{h}}^\top \\ \cdots \\ \frac{\partial d}{\partial \mathbf{z}}^\top \end{pmatrix} \tag{12}$$

where $\Lambda_{\mathbf{h}}$ is the 9×9 covariance of the homography and $\Lambda_{\mathbf{x}_1}$ and $\Lambda_{\mathbf{x}_2}$ are the 2×2 covariance matrices of the input image points.

8 Examples and applications

The correctness of the uncertainty analysis is demonstrated in this section on a number of examples. It is shown that the ground truth measurements always lie within the estimated error bounds. Furthermore, the utility of the analysis is illustrated. The covariance expression *predicts* uncertainty given the number of image-world computation points and their distribution. It is thus possible to decide where correspondences are required in order to achieve a particular desired measurement accuracy.

In all of the following error is assumed to be in both computation points and measurement points.

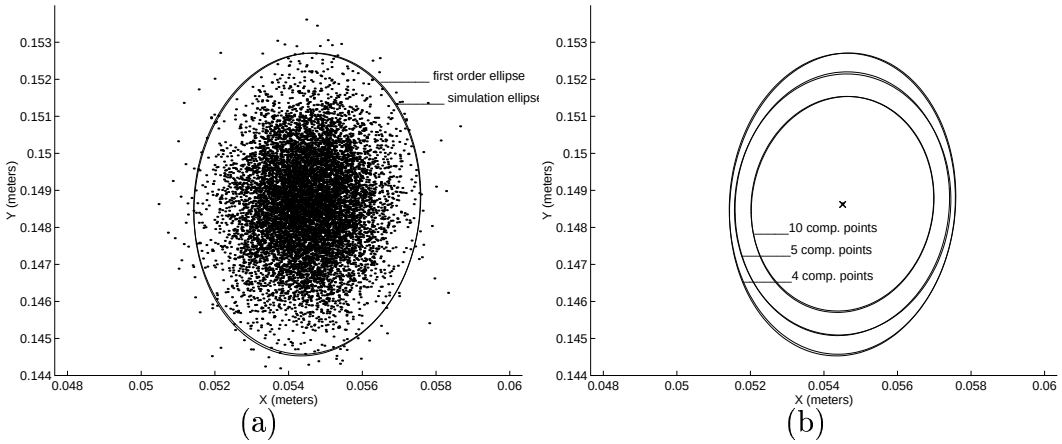


Fig. 3. **Uncertainty in point localization:** (a) `H` is computed from the theory of sections 3.4 and 5 using only 4 noisy computation points. 10000 image points are randomly generated from a Gaussian distribution centred on an image test point $\bar{x}$ and then backprojected onto the world plane. The statistical covariance ellipse of the world points is computed and plotted together with the predicted one. 3 std. dev. are visualised for each uncertainty ellipse - (b) The first order and simulated uncertainty ellipse's area decreases as the number of computation points increase from 4 to 5 to 10 as expected from the theory.

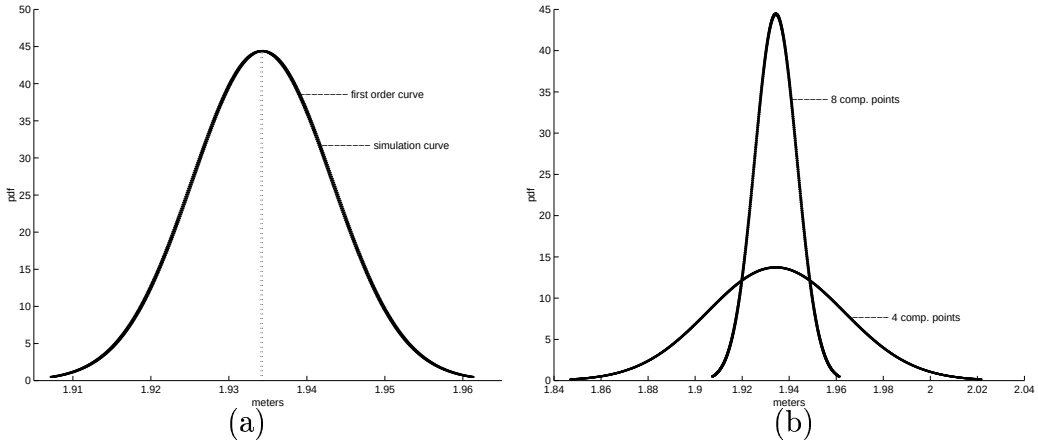


Fig. 4. **Uncertainty in distance measurement:** (a) `H` is computed from the theory of sections 3.4 and 5 using only 4 noisy computation points. 10000 image points are randomly generated from a Gaussian distribution centred on an image test point $\bar{x_1}$ and another 10000 points generated from a Gaussian distribution centred on another image test point $\bar{x_2}$. The points are backprojected onto the world plane and the distances between the pairs are computed. The statistical distribution of the distances is computed and plotted together with the predicted one. 3 std. dev. are visualised for each curve - (b) The first order and simulated uncertainties decrease as the number of computation points increase from 4 to 8.

8.1 Theory validation using Monte Carlo analysis

In order to illustrate the accuracy in point localization of this first order error propagation analysis we show, in figure 3, a comparison between the covariance

ellipse obtained by the first order analysis and the one obtained by a Monte-Carlo evaluation of the actual non-linear homography mapping. The predicted ellipse and the simulated one are virtually indistinguishable.

Figure 4, demonstrates the uncertainty in distance measurements. A comparison between the the gaussian distribution obtained by the first order analysis and, again, the distribution obtained by a Monte-Carlo evaluation of the non-linear homography mapping is shown. The predicted curve and the simulated one are again indistinguishable.

Figures 3 and 4 are obtained using suitable parameters for images of real scenes.

8.2 Uncertainty in point localization

8.2.1 Varying the location of the computations points.

Figure 5 shows an example of an indoor scene. Figure 5a is the original image and in figures 5b-d this image is back-projected onto the world plane by the computed homography. The `H` matrix is computed using four computations points in all cases. The standard deviations used for the computation are $\sigma = 1\,pixel$ in the image and $\Sigma = 0.5\,cm$ in the world.

Three test points are shown with their uncertainty ellipses. Note that as the distance of the test point to computation points increases, the uncertainty increases. More spatially homogeneous uncertainties are achieved by distributing the computation points across the scene.

8.2.2 Varying the number of computation points.

Figure 6 shows the same scene as before. Figure 5a is the original image and figures 5b-d are the unskewed ones.

The `H` matrix is computed using four points in figure 5b, six point in figure 5c and eight points in figure 5d. The standard deviations used for the computation are as before $\sigma = 1\,pixel$ in the image and $\Sigma = 0.5\,cm$ in the world.

The same three test points are shown with their uncertainty ellipses. Smaller uncertainties are achieved by increasing the number of computation points.

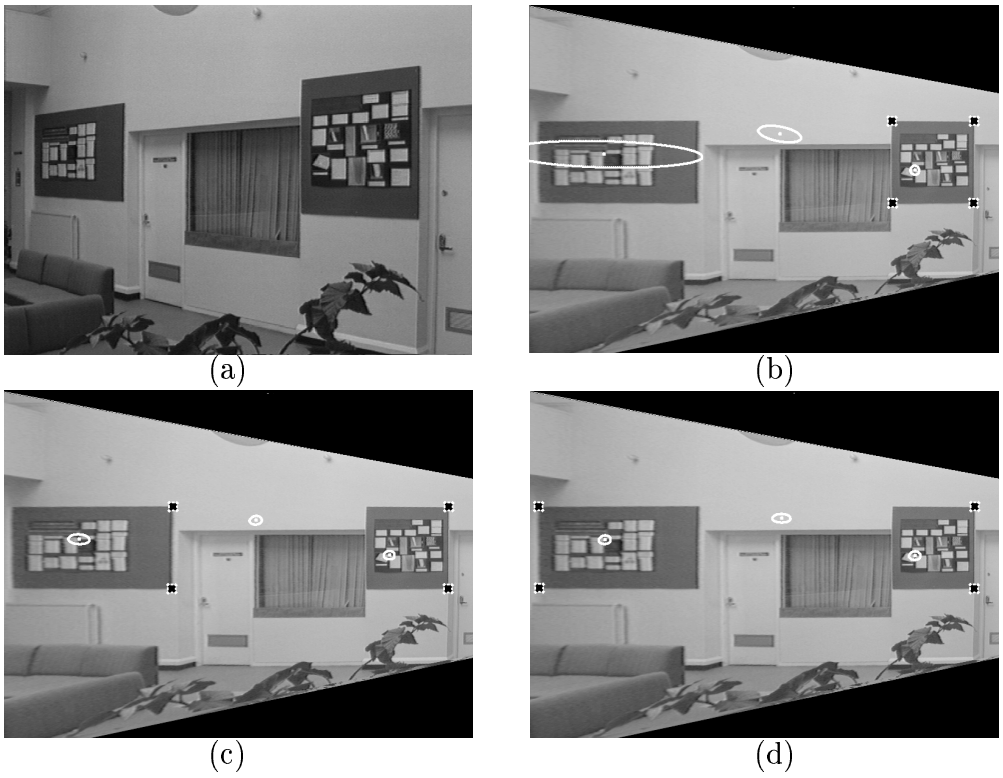


Fig. 5. (a) Original image. (b-d) projectively unskewed back-projection. The computation points used to estimate `H` are marked by black asterisks. The uncertainty ellipses shown for test points are at the 9 std. dev. level for clarity.

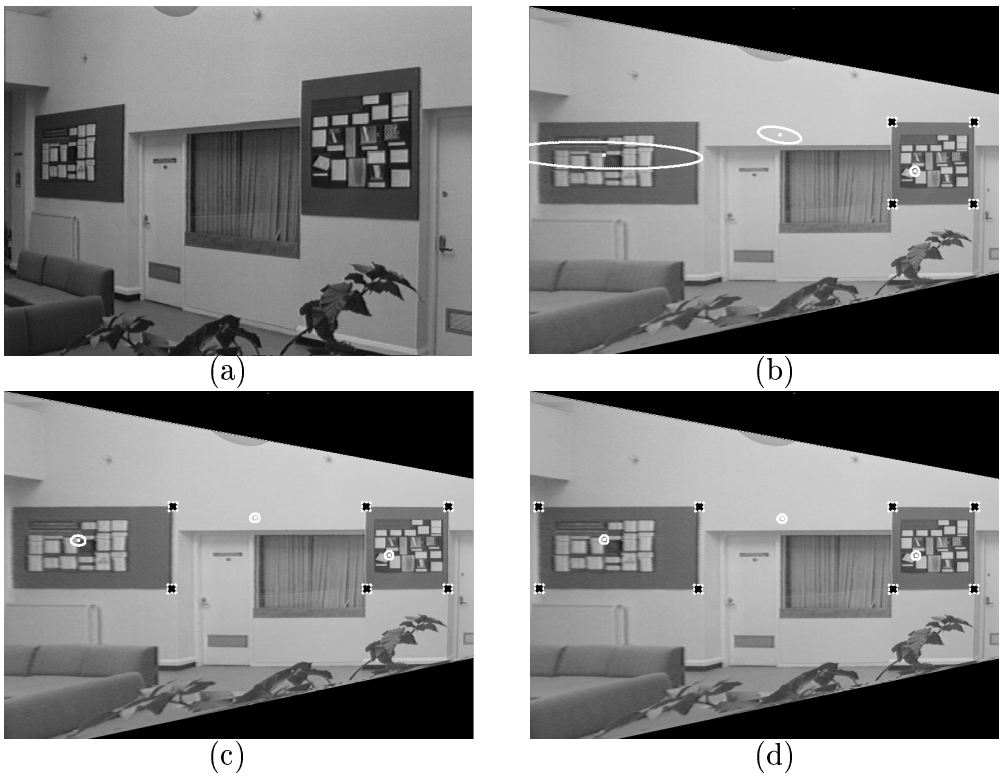


Fig. 6. (a) Original image. (b-d) projectively unskewed back-projection. The computation points used to estimate `H` are marked by black asterisks. The uncertainty ellipses shown for test points are at the 9 std. dev. level for clarity.

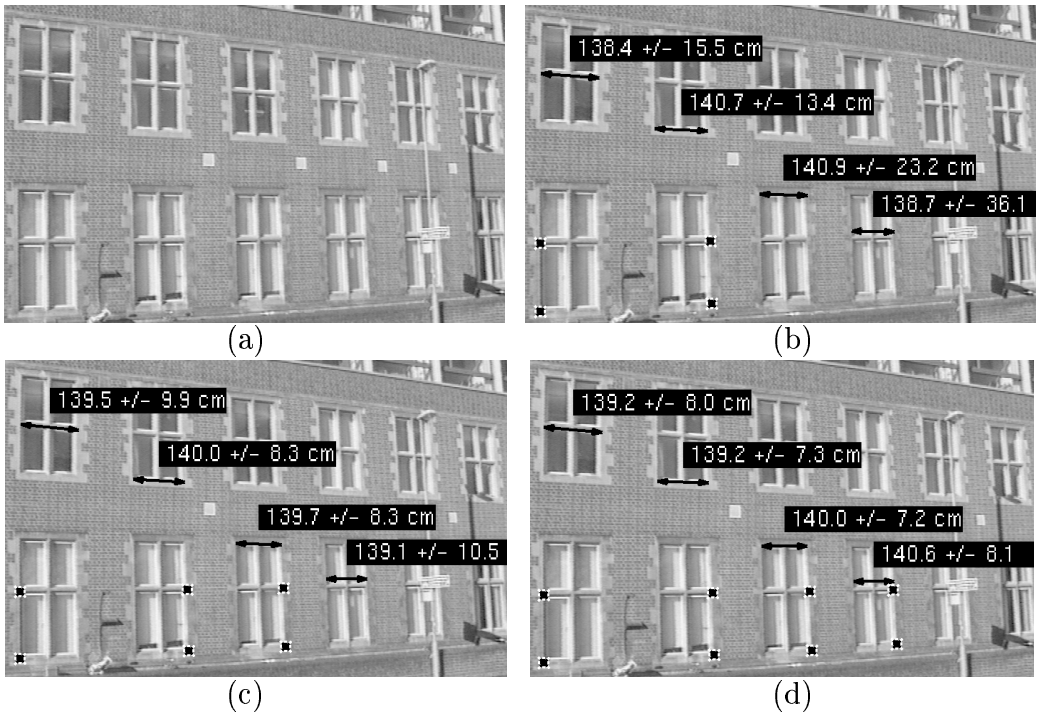


Fig. 7. (a) Original image. (b-d) length measurements based on a homography computed from the points marked by black asterisks. The uncertainty bound is ±3 std. dev. The actual width is 139 cm.

8.3 Uncertainty in distance measurement

8.3.1 Varying the number of computation points.

Figure 7b-d shows length measurements for a homography computed from four, six and eight correspondences. The standard deviations used for the computation are $\sigma = 1$ *pixel* and $\Sigma = 1$ *cm*. Again measurements further from the computation point have a larger uncertainty. Increasing the number of computation points decreases all the uncertainties. Note that all the measurement ranges computed include the ground truth width (139 cm).

8.3.2 Distance between parallel lines.

Figure 8 illustrates the computation of pairs of parallel world lines and the measurement of their distances.

In the image a line is selected, and the one parameter family of lines parallel to it on the world plane are computed from the estimated $\mathbf{H}$.

Given a line $\mathbf{l}$ and a point $\mathbf{p}$ in the image we want to find the line $\mathbf{l}'$ through $\mathbf{p}$ whose projection $\mathbf{L}'$ is parallel to the projection of $\mathbf{l}$ into the world plane.



(a) (b)

Fig. 8. Crystallography Labs Oxford. (a) Original image. (b) Measurement of distances between two pairs of parallel lines (in the world). The four computation points used are marked by black asterisks. The uncertainty bound is ± 3 std. dev. The actual height of upper and lower windows is 174 cm.

This is simply $\mathbf{l}' = \mathbf{p} \times \mathbf{v}$ where $\mathbf{v}$ is the vanishing point for that direction, and $\mathbf{v}$ is given by: $\mathbf{v} = \mathtt{H}^{-1}\mathtt{R}\mathtt{H}^{-\top}\mathbf{l}$ with

$$\mathtt{R} = \begin{pmatrix} 0 & 1 & 0 \\ -1 & 0 & 0 \\ 0 & 0 & 0 \end{pmatrix}$$

Once a pair of lines $\mathbf{l}, \mathbf{l}'$ is selected their distance can be easily computed.

In figure 8 the ground truth lies within the computed measurement range.

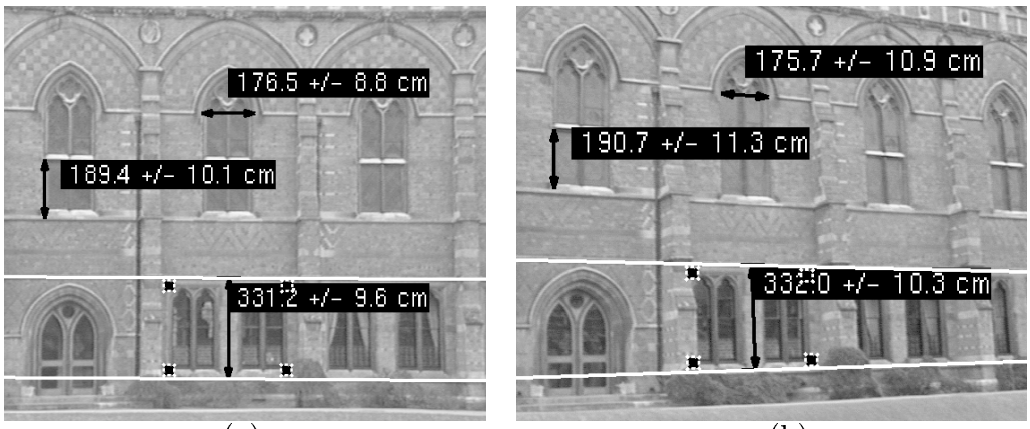
8.3.3 Different views, same computation points.

Figure 9 illustrates that the uncertainties also depend on the viewpoint. In both cases the ground truth lies within the predicted measurement range, but this range is larger in the view with more severe perspective distortion (fig. 9b).

Measurements of distances between two points and between parallel world lines are demonstrated.

9 Conclusion and extensions

We have developed a first order model of uncertainty prediction which takes account of all the errors involved in estimating the homography and employing it for measurements. The validity has been demonstrated in a number of



(a) (b)

Fig. 9. Keble College Oxford. The computation points are the same, but the viewpoint distortion is more severe in (b). This is reflected in the larger uncertainties. The uncertainty bound is 3 std. dev.. The actual width of the upper windows is 176 cm. Note the computed parallel lines.

applications. The approach can be applied to any world measurement, lengths and parallelism have been demonstrated, and area and angles can also be computed.

It is worth noting that although the theory has been developed here for plane to plane homographies, the same approach can be used for line to line and 3-space to 3-space homographies. In particular the matrix perturbation based derivation of covariance can be used where these relations are estimated from an equation of the form $\mathbf{A}\mathbf{h} = \mathbf{0}$. This includes estimating epipolar geometry.

We are currently extending these ideas in several ways:

(1) The uncertainty in the homography depends on the uncertainty in the computation points and on the algorithm used to compute the homography itself. In this paper the homogeneous solution (section 3) has been employed and the covariance associated with the homography computed (section 5). We are now investigating how to estimate the uncertainty for the non-linear geometric solution.
(2) Errors arise if the computation points in the world do not all lie on the same plane. It is not possible to detect non-planarity from a single view, but if two views are used then a "plane plus parallax" [3,8] approach can be used to detect automatically and discard the correspondences not lying on the reference plane.
(3) The camera has so far been modeled as a perfect perspective mapping. However, if small focal lengths are used then radial distortion effects appear in the acquired images. Radial distortion can affect the performance of our system considerably and, therefore, methods to correct the image are being investigated.
(4) Mismatching image-world correspondences badly affect the computed ho-

mography. A method to check the consistency of the computation pairs is, therefore, necessary. A RANSAC [6] like approach can be employed automatically to detect and reject inconsistent pairs if more than the minimal set (four) are available.

Acknowledgements.

We would like to thank Andrew Fitzgibbon for the development and maintenance of the Targetjr/IUE software. This software was supported financially by the UK EPSRC IUE Implementation Project GR/L05969.

References

[1] J. C. Clarke. Modelling uncertainty: A primer. Technical Report 2161/98, University of Oxford, Dept. Engineering Science, 1998.

[2] H. Cramer. *Mathematical Methods of Statistics.* Princeton Univ. Press., 1946.

[3] A. Criminisi, I. Reid, and A. Zisserman. Duality, rigidity and planar parallax. In *Proc. European Conference on Computer Vision*, 1998.

[4] G. Csurka, C. Zeller, Z. Zhang, and O. Faugeras. Characterizing the uncertainty of the fundamental matrix. Technical Report 2560, I.N.R.I.A., France, 1995.

[5] O. Faugeras. *Three-Dimensional Computer Vision: a Geometric Viewpoint.* MIT Press, 1993.

[6] M. A. Fischler and R. C. Bolles. Random sample consensus: A paradigm for model fitting with applications to image analysis and automated cartography. *Comm. Assoc. Comp. Mach.*, 24(6):381–395, 1981.

[7] G. H. Golub and C.F. Van Loan. *Matrix Computations.* The John Hopkins University Press, Baltimore, MD, second edition, 1989.

[8] M. Irani, P. Anandan, and D. Weinshall. From reference frames to reference planes: Multi-view parallax geometry and applications. In *Proc. European Conference on Computer Vision*, 1998.

[9] J. Mundy and A. Zisserman. *Geometric Invariance in Computer Vision.* MIT Press, 1992.

[10] W. Press, B. Flannery, S. Teukolsky, and W. Vetterling. *Numerical Recipes in C.* Cambridge University Press, 1988.

[11] I. Reid and A. Zisserman. Goal-directed video metrology. In R. Cipolla and B. Buxton, editors, *Proc. 4th European Conference on Computer Vision, LNCS 1065, Cambridge*, volume II, pages 647–658. Springer, April 1996.

[12] J. A. Rice. *Mathematical Statistics and Data Analysis.* Wadsworth and Brooks, California, 1988.

[13] J. Semple and G. Kneebone. *Algebraic Projective Geometry.* Oxford University Press, 1979.

[14] K. A. Stroud. *Engineering Mathematics.* MacMillan Education, 3rd edition, 1987.

[15] P. H. S. Torr and A. Zisserman. Robust parameterization and computation of the trifocal tensor. *Image and Vision Computing*, 15:591–605, 1997.

[16] J. Weng, T. S. Huang, and N. Ahuja. Motion and structure from two perspective views: algorithms, error analysis and error estimation. *IEEE Trans. on Patt. Analysis and Machine Intelligence*, 11(5):451–476, 1989.

[17] Z. Zhang, R. Deriche, O. Faugeras, and Q. Luong. A robust technique for matching two uncalibrated images through the recovery of the unknown epipolar geometry. *Artificial Intelligence*, 78:87–119, 1995.